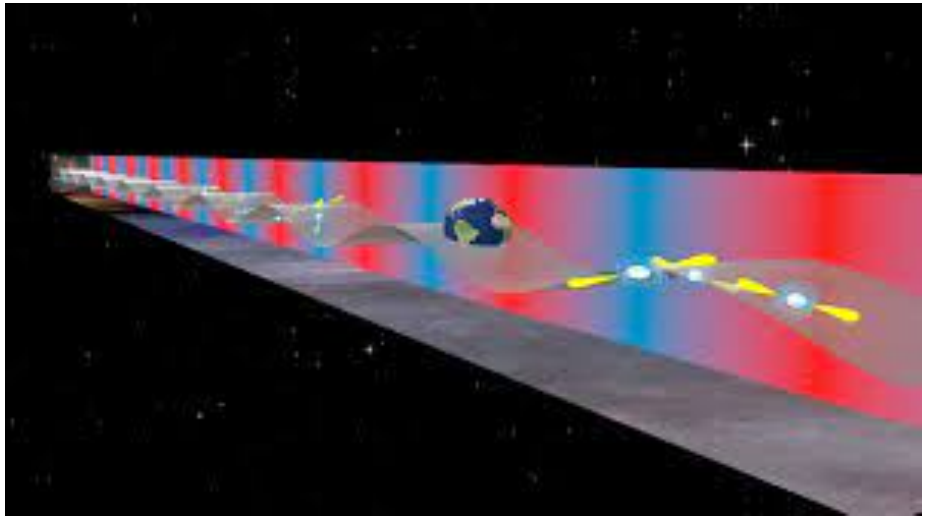

Can we observe the QCD phase transition-generated gravitational waves through pulsar timing arrays?

Tina Kahniashvili
Carnegie Mellon University, USA & Ilia State University, Georgia

In collaboration with:
Axel Brandenburg, Emma Clarke, Yutong He
arXiv: 2102.12428

PHENO2021
May 25, 2021

outline

- ✓ NANOGrav signal possible sources:
  - QCD energy scales
- ✓ Gravitational waves from primordial turbulence
- ✓ Numerical simulations
- ✓ What is next?

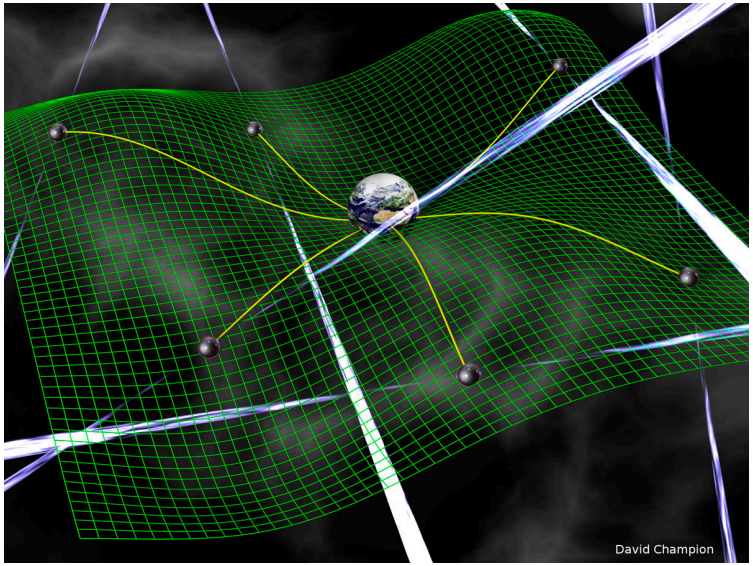

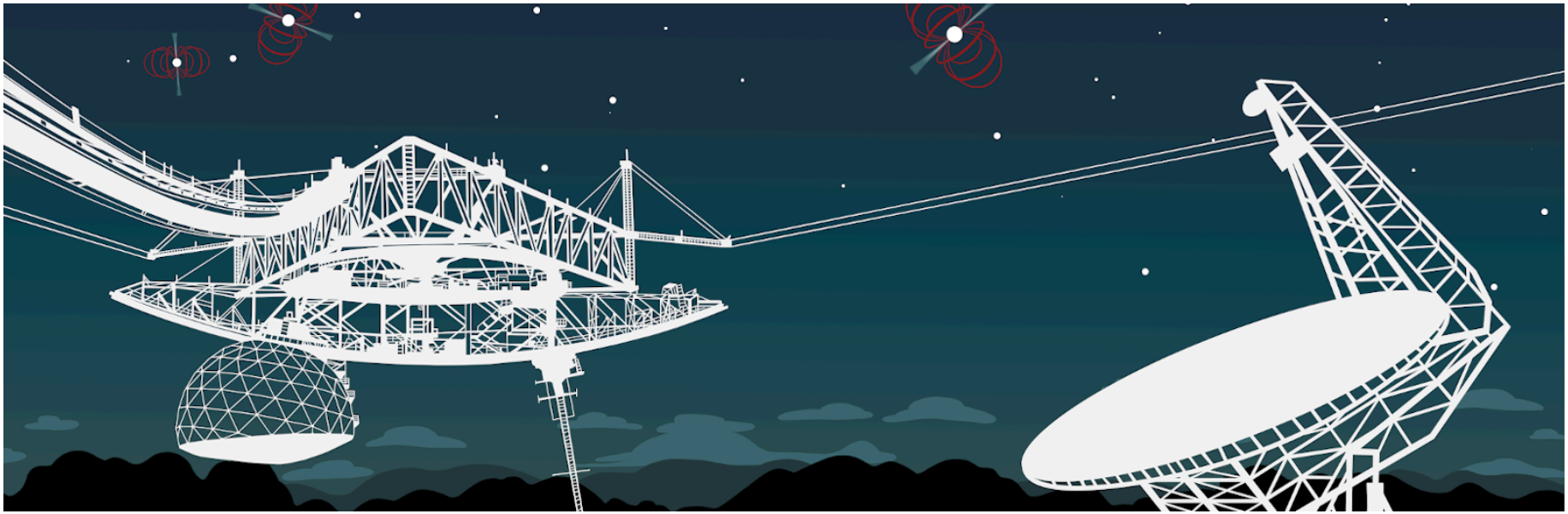

gravitational waves: basics

$$g_{\mu\nu} = \eta_{\mu\nu} + h_{\mu\nu}$$

$$R_{\mu\nu} - \frac{1}{2} g_{\mu\nu} R = \frac{8\pi G}{c^4} T_{\mu\nu}$$

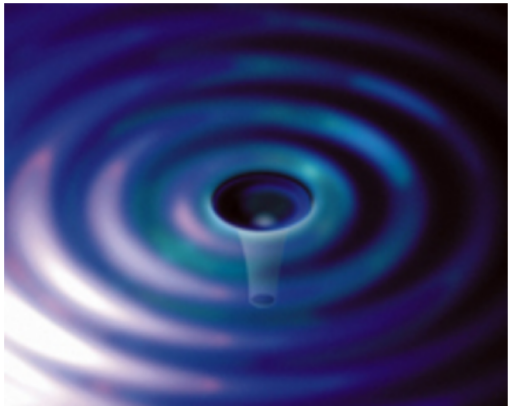

Mukhanov, et al. 1992

- ✓ Ripples of space-time
- ✓ No analogy in Newtonian physics
- ✓ Gauge-invariant perturbations
- ✓ Two degrees of Freedom (3x3)
  - Symmetric $h_{ij}=h_{ji}$ (6 terms)
  - Traceless $h_i^i = 0$ (5 terms)
  - Transverse $h_{ij}\, k^j = 0$ (2 terms)

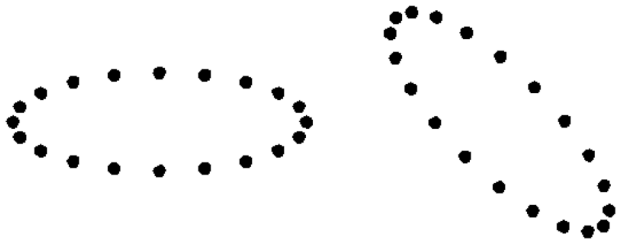

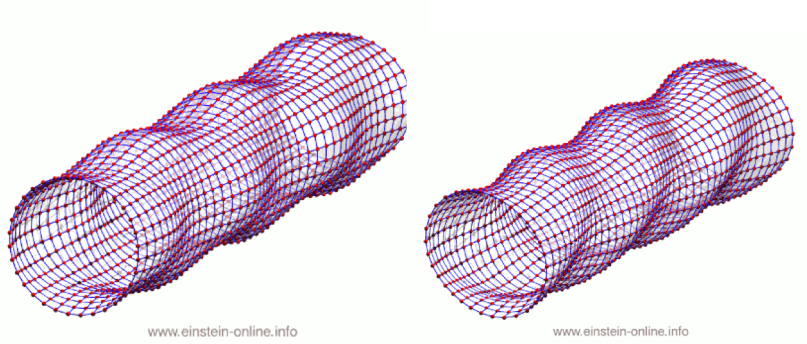

Gravitational waves are polarized due to the nature of their source.

NANOGrav 12.5 years observations:

$$h_c(f) = A_{\rm CP}\left(\frac{f}{f_{\rm yr}}\right)^{\alpha_{\rm CP}},$$

NANOGrav 12.5-year sensitivity range of 1–100 nHz

Broken PL 5 frequency 30-frequency

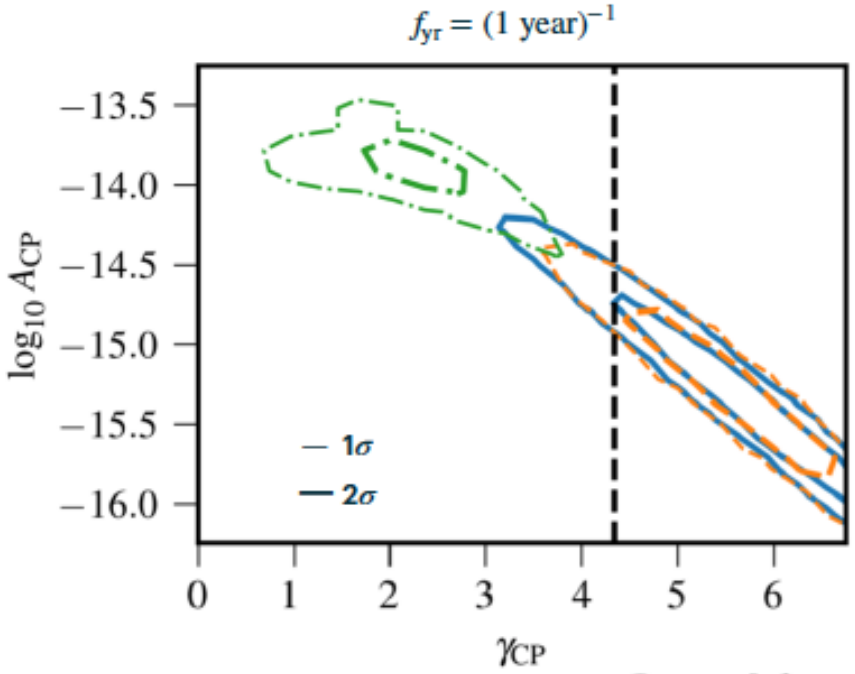

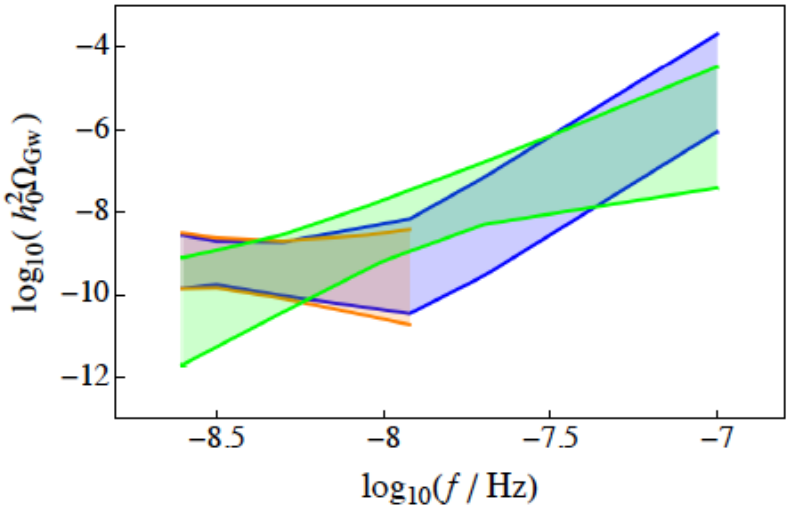

Credit; Emma Clarke

Arzoumanian et al (2020)

$$\mathcal{E}_{\rm GW}(t) = \frac{1}{32\pi G}\langle \dot{h}^{\rm TT}_{ij,\rm phys}(\mathbf{x},t)\dot{h}^{\rm TT}_{ij,\rm phys}(\mathbf{x},t)\rangle$$

$$\Omega_{\rm GW}(t,f) = \frac{1}{\mathcal{E}_{\rm crit}(t)}\frac{{\rm d}\mathcal{E}_{\rm GW}}{{\rm dln}f}$$

$$\Omega_{\rm GW}(f) = \frac{2\pi^2}{3H_0^2}f^2h_c^2(f) = \Omega^{\rm yr}_{\rm GW}\left(\frac{f}{f_{\rm yr}}\right)^{5-\gamma_{\rm CP}}$$

possible sources:

Astrophysical:

✓ Super massive black hole binary (SMBHB) (Phinney 2001): γ=13/3

Cosmological:

✓ Bubbles collisions (Kosowsky et. Al. 1993)
✓ Inflation (Vagnozzi 2021)
✓ Cosmic strings (Blanco-Pillado et al. 2021)
✓ Seed magnetic fields (Neronov et. Al. 2021)
✓ Hydrodynamic and MHD Turbulence (Brandenburg et al. 2021)

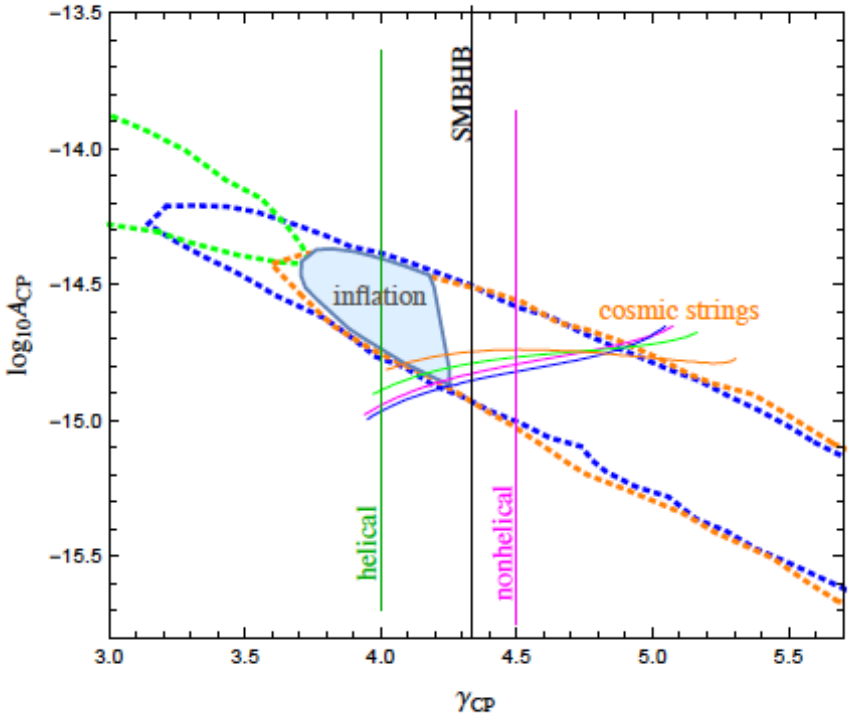

Credit: Emma Clarke

QCD energy scale

$$\frac{a_0}{a_\star} = 10^{12}\left(\frac{g_{S,\star}}{15}\right)^{\frac{1}{3}}\left(\frac{T_\star}{150\ \mathrm{MeV}}\right)$$

$$H_\star^2 = \frac{8\pi G}{2}\mathcal{E}_{\mathrm{rad},\star} \qquad \mathcal{E}_{\mathrm{rad},\star} = \frac{\pi^2 g_\star}{30}T_\star^4 \qquad (c = k_B = \hbar = 1)$$

$$f_H \simeq (1.8\times10^{-8}\mathrm{Hz})10^{12}\left(\frac{g_\star}{15}\right)^{\frac{1}{3}}\left(\frac{T_\star}{150\ \mathrm{MeV}}\right)$$

gravitational waves from phase transitions

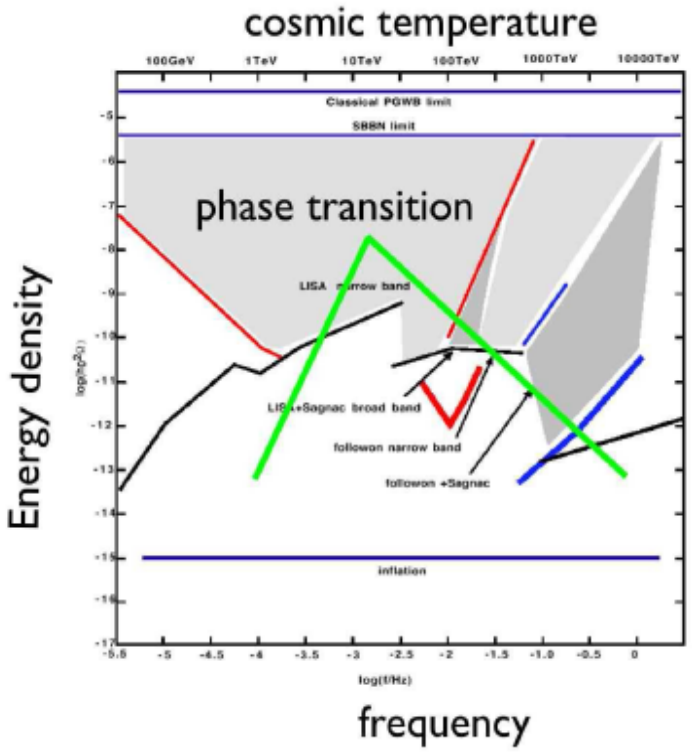

C. Hogan, 2006

Pioneering works:

- Winicour 1973
- Hogan 1982, 1986
- Turner & Wilczek 1990
- Kosowsky, Turner, Watkins. 1992
- Kosowsky & Turner 1993
- Kamionkowski et al. 1994

Crossover: beyond-SM physics:
axion-driven turbulence, Miniati et al. 2018

First order phase transitions?

VOLUME 69, NUMBER 14 PHYSICAL REVIEW LETTERS 5 OCTOBER

Gravitational Waves from First-Order Cosmological Phase Transitions

Arthur Kosowsky,[1],[2] Michael S. Turner,[1],[2],[3] and Richard Watkins[1],[3]
[1]*NASA/Fermilab Astrophysics Center, Fermi National Accelerator Laboratory, Batavia, Illinois 60510-0500*
[2]*Department of Physics, Enrico Fermi Institute, The University of Chicago, Chicago, Illinois 60637-1433*
[3]*Department of Astronomy & Astrophysics, Enrico Fermi Institute, The University of Chicago, Chicago, Illinois 60637*
(Received 6 December 1991; revised manuscript received 26 May 1992)

A first-order cosmological phase transition that proceeds through the nucleation and collision of true-vacuum bubbles is a potent source of gravitational radiation. Possibilities for such include first-order inflation, grand-unified-theory-symmetry breaking, and electroweak-symmetry breaking. We have calculated gravity-wave production from the collision of two scalar-field vacuum bubbles, and, using an approximation based upon these results, from the collision of 20 to 30 vacuum bubbles. We present estimates of the relic background of gravitational waves produced by a first-order phase transition; in general, $\Omega_{GW} \sim 10^{-9}$ and $f \sim (10^{-6}\ \mathrm{Hz})(T/1\ \mathrm{GeV})$.

gravitational waves from anisotropic stresses

Mon. Not. R. astr. Soc. (1987) **229**, 357–370

$$\ddot{h}_{ij} + 2\frac{\dot{a}}{a}\dot{h}_{ij} - \Delta h_{ij} = -\frac{16\pi G}{c^4} a^2(\eta)\,\delta T_{ij}.$$

Generation of gravitational waves by the anisotropic phases in the early Universe

Magnetic fields;
Turbulence (hydro & MHD)

D. V. Deryagin, D. Yu. Grigoriev and V. A. Rubakov *Institute for Nuclear Research, USSR Academy of Sciences, Moscow 117312, USSR*

M. V. Sazhin *P. K. Sternberg Astronomical Institute, Universitetskii pr. 13, Moscow 119899, USSR*

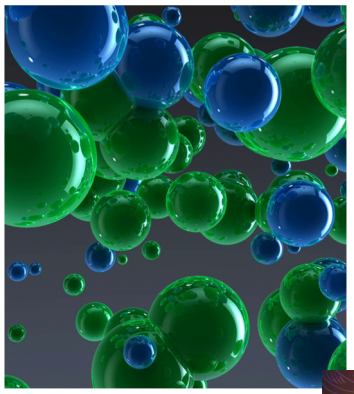

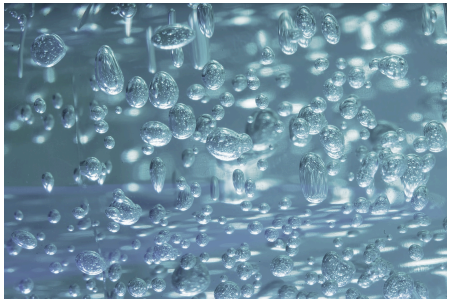

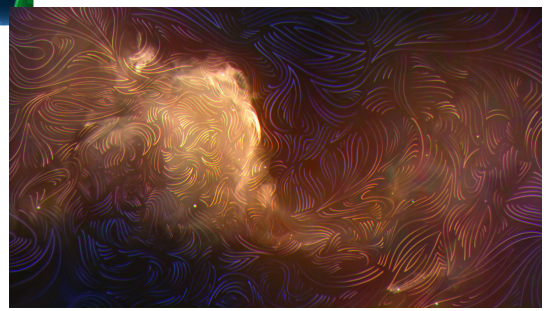

The space interferometer will be a unique device to observe the gravitational radiation from anisotropic phases possible at the energy scales T=1TeV-100GeV.

Pulsar Timing Array (PTA) are sensible to gravitational waves generated or present at QCD energy scales

gravitational waves primordial turbulence?

$$\nabla^2 \delta\rho(\boldsymbol{x},t) - \frac{1}{c_s^2}\frac{\partial^2}{\partial t^2}\delta\rho(\boldsymbol{x},t) = -\frac{\partial^2}{\partial x_i \partial x_j} T(\boldsymbol{x},t) \qquad c = 1$$

$$\nabla^2 h_{ij}(\boldsymbol{x},t) - \frac{\partial^2}{\partial t^2} h_{ij}(\boldsymbol{x},t) = -16\pi G\, S_{ij}(\boldsymbol{x},t) \qquad c_s^2 = \frac{\delta p}{\delta \rho}$$

Aero-acoustic approximation:

- ✓ sound waves generation by turbulence
- ✓ Gravitational waves generation

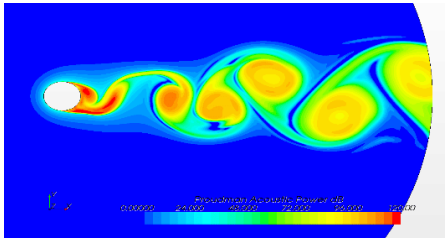

Lighthill, 1952; Proudman 1952

Kosowsky, Mack, Kahniashvili, 2002
Dolgov, Grasso, Nicolis, 2002
Gogoberidze, Kahniashvili, Kosowsky, 2002

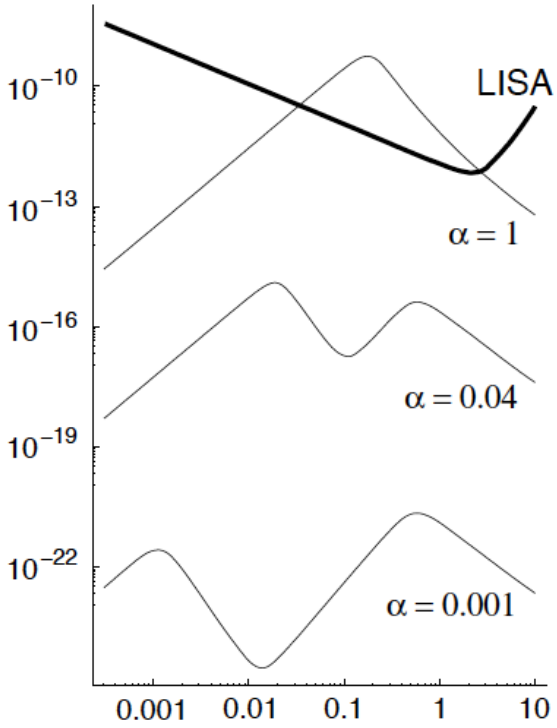

Nicolis 2004

why primordial turbulence?

Bubble nucleations

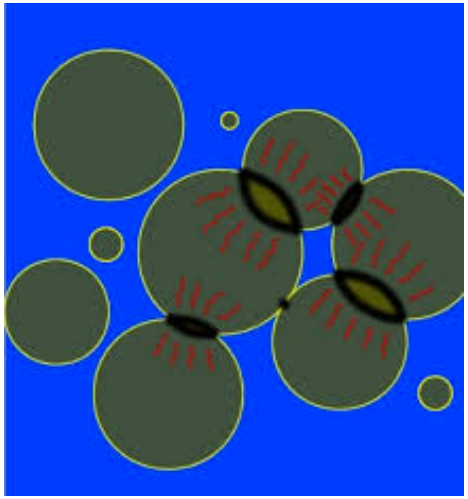

Baym et al. 1995

Magnetic fields

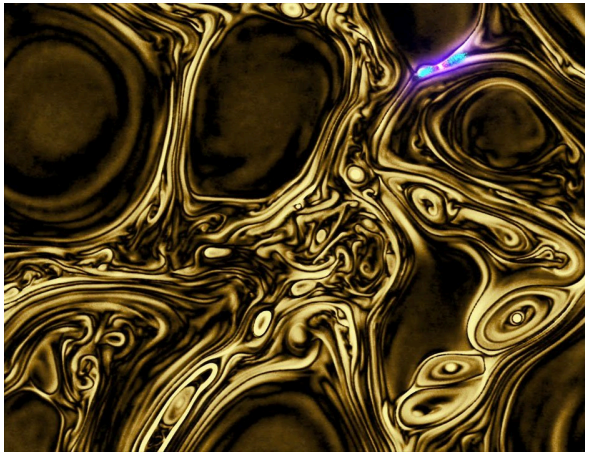

Quashnock, et al. 1989

- ✓ Injection of the magnetic energy at a given scale (phase transition bubble)
- ✓ Coupling of the magnetic field with primordial plasma

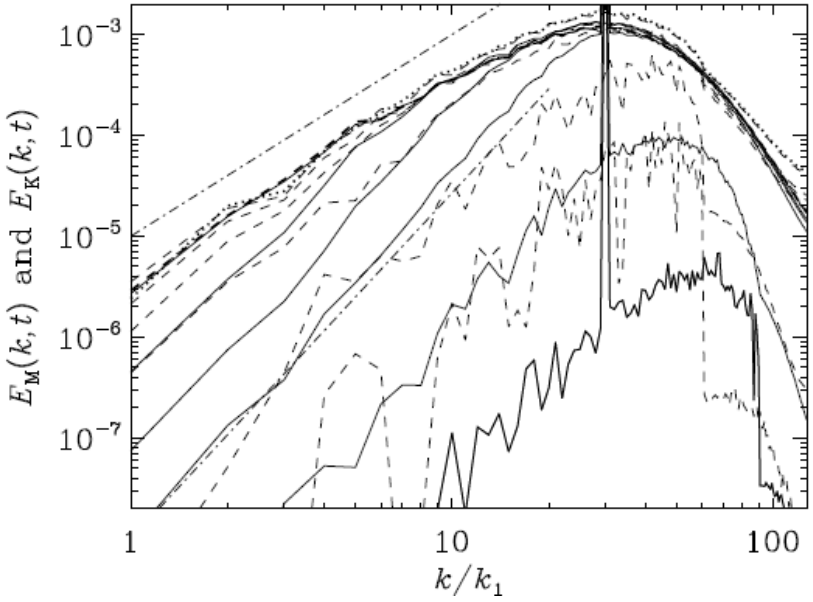

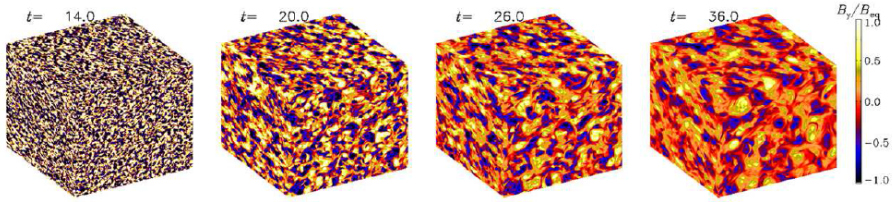

FIG. 2: Evolution of the turbulent magnetic field after turning off the forcing at time $t = 14\,t_1$. The B_y component is shown on the periphery of the computational domain.

Kahniashvili, et al. 2010

why primordial magnetic fields?

E ASTROPHYSICAL JOURNAL LETTERS, 727:L4 (4pp), 2011 January 20 doi:10.1088/2041-8205/727/1/L4

LOWER LIMIT ON THE STRENGTH AND FILLING FACTOR OF EXTRAGALACTIC MAGNETIC FIELDS

K. DOLAG[1,2], M. KACHELRIESS[3], S. OSTAPCHENKO[3,4], AND R. TOMÀS[5]
[1] Universitätssternwarte München, München, Germany
[2] Max-Planck-Institut für Astrophysik, Garching, Germany
[3] Institutt for fysikk, NTNU, Trondheim, Norway
[4] D. V. Skobeltsyn Institute of Nuclear Physics, Moscow State University, Moscow, Russia
[5] II. Institut für Theoretische Physik, Universität Hamburg, Germany
Received 2010 September 16; accepted 2010 November 25; published 2010 December 21

ABSTRACT

High-energy photons from blazars can initiate electromagnetic pair cascades interacting with the extragalactic photon background. The charged component of such cascades is deflected and delayed by extragalactic magnetic fields (EGMFs), thereby reducing the observed point-like flux and potentially leading to multi-degree images in the GeV energy range. We calculate the fluence of 1ES 0229+200 as seen by *Fermi*-LAT for different EGMF profiles using a Monte Carlo simulation for the cascade development. The non-observation of 1ES 0229+200 by *Fermi*-LAT suggests that the EGMF fills at least 60% of space with fields stronger than $\mathcal{O}(10^{-16}$ to $10^{-15})$ G for lifetimes of TeV activity of $\mathcal{O}(10^2$ to $10^4)$ yr. Thus, the (non-)observation of GeV extensions around TeV blazars probes the EGMF in voids and puts strong constraints on the origin of EGMFs: either EGMFs were generated in a space filling manner (e.g., primordially) or EGMFs produced locally (e.g., by galaxies) have to be efficiently transported to fill a significant volume fraction as, e.g., by galactic outflows.

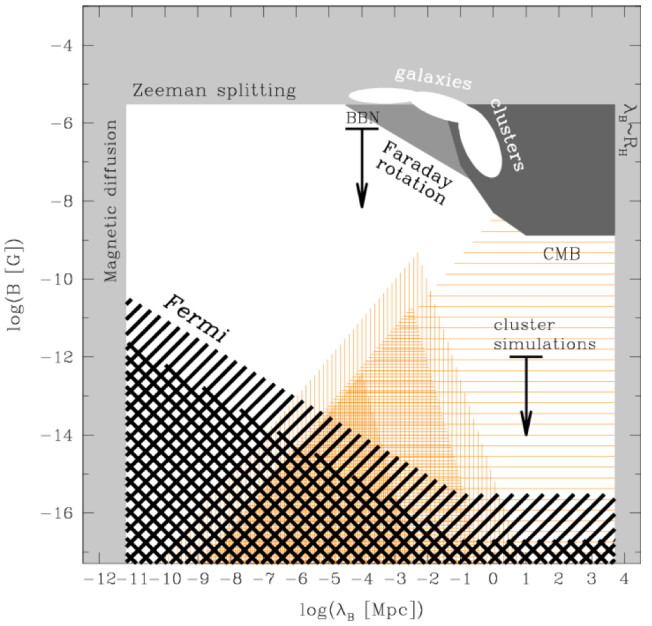

Neronov and Vovk 2010

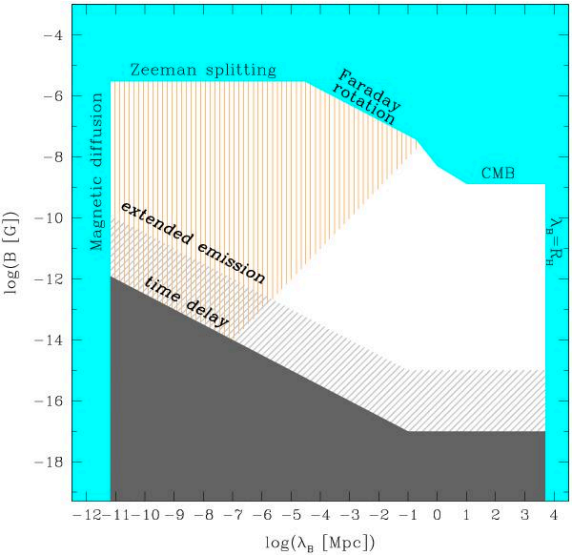

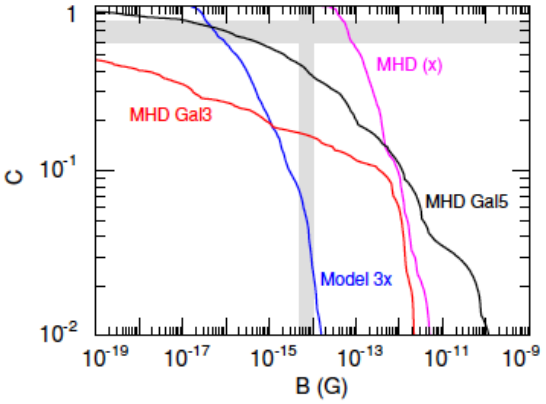

Figure 4. Cumulative volume filling factor $C(B)$ for the four different EGMF models found in MHD simulations.
(A color version of this figure is available in the online journal.)

4. SUMMARY

We have calculated the fluence of 1ES 0229+200 as seen by *Fermi*-LAT using a Monte Carlo simulation for the cascade development. We have discussed the effect of different EGMF profiles on the resulting suppression of the point-like flux seen by *Fermi*-LAT. Since the electron cooling length is much smaller than the mean free path of the TeV photons, a sufficient suppression of the point-like flux requires that the EGMF fills a large fraction along the line of sight toward 1ES 0229+200, $f \gtrsim 0.6$. The lower limit on the magnetic field strength in this volume is $B \sim \mathcal{O}(10^{-15})$ G, assuming 1ES 0229+200 is stable at least for 10^4 yr, weakening by a factor of 10 for $\tau = 10^2$ yr. These limits put very stringent constraints on the origin of EGMFs. Either the seeds for EGMFs have to be produced by a volume filling process (e.g., primordial) or very efficient transport processes have to be present which redistribute magnetic fields that were generated locally (e.g., in galaxies) into filaments and voids with a significant volume filling factor.

different magnetogenesis probes

- Gravitational waves propagate almost freely and retain the information about the source and physical processes
  - Frequency determines the source characteristic length scale
  - Amplitudes – the source efficiency and energetics.

$$f_{GW} = 2/l_s \qquad \Omega_{GW} \sim \Omega_B^2$$

$$N_b = \frac{H^{-1}}{l_s}$$

magnetic fields at recombination

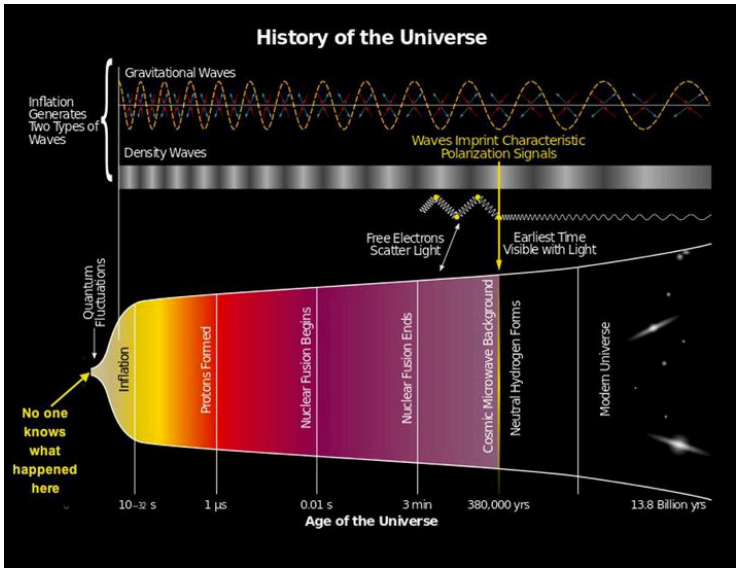

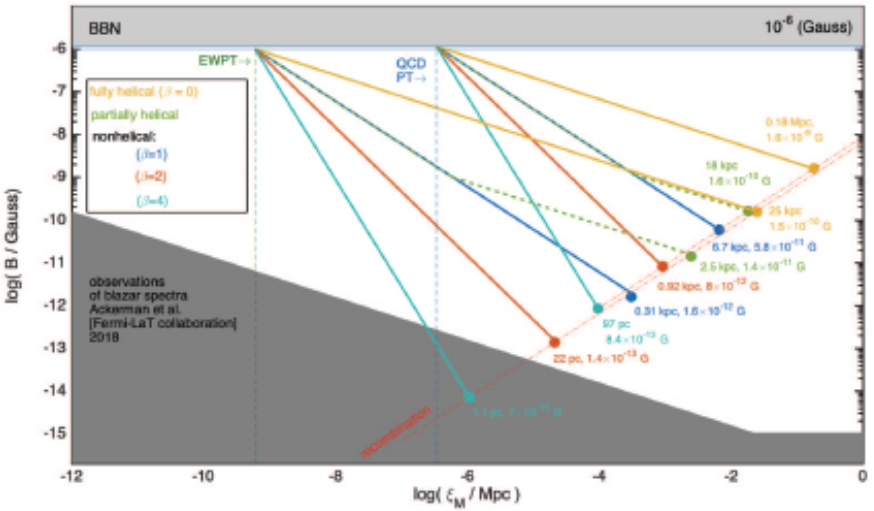

Credit: Emma Clarke

numerical simulations

- ✓ To account properly non-linear processes (MHD)
- ✓ Not be limited by the short duration of the phase transitions
- ✓ Two stages turbulence decay
  - Forced turbulence
  - Free decay
- ✓ The source is present till recombination (after the field is frozen in)
- ✓ Results – strongly initial conditions dependent

$$\left(\frac{\partial^2}{\partial t^2} - c^2\nabla^2\right) h_{ij}^{\rm TT} = \frac{16\pi G}{a^3 c^2} T_{ij}^{\rm TT},$$

$$h_{ij}^{\rm TT} = a h_{ij}^{\rm TT,phys} \qquad {\rm d}t_{\rm phys} = a{\rm d}t$$

Grishchuk 1974

$$\frac{\partial \ln\rho}{\partial t} = -\frac{4}{3}\left(\boldsymbol{\nabla}\cdot\boldsymbol{u} + \boldsymbol{u}\cdot\boldsymbol{\nabla}\ln\rho\right) + \frac{1}{\rho}\left[\boldsymbol{u}\cdot(\boldsymbol{J}\times\boldsymbol{B}) + \eta\boldsymbol{J}^2\right],$$

$$\frac{\partial \boldsymbol{u}}{\partial t} = -\boldsymbol{u}\cdot\boldsymbol{\nabla}\boldsymbol{u} + \frac{\boldsymbol{u}}{3}\left(\boldsymbol{\nabla}\cdot\boldsymbol{u} + \boldsymbol{u}\cdot\boldsymbol{\nabla}\ln\rho\right) + \frac{2}{\rho}\boldsymbol{\nabla}\cdot(\rho\nu\mathsf{S}) - \frac{1}{4}\boldsymbol{\nabla}\ln\rho - \frac{\boldsymbol{u}}{\rho}\left[\boldsymbol{u}\cdot(\boldsymbol{J}\times\boldsymbol{B}) + \eta\boldsymbol{J}^2\right] + \frac{3}{4\rho}\boldsymbol{J}\times\boldsymbol{B},$$

$$\frac{\partial \boldsymbol{B}}{\partial t} = \boldsymbol{\nabla}\times(\boldsymbol{u}\times\boldsymbol{B} - \eta\boldsymbol{J} + \boldsymbol{\mathcal{F}}), \quad \boldsymbol{J} = \boldsymbol{\nabla}\times\boldsymbol{B}.$$

$$\mathcal{E}_{\rm M}(t) = \mathcal{E}_{\rm M}^{\rm max}\left(1 + \Delta t/\tau\right)^{-p} \qquad \mathcal{E}_{\rm GW}^{\rm sat} = \left(q\mathcal{E}_{\rm M}^{\rm max}/k_{\rm f}\right)^2$$

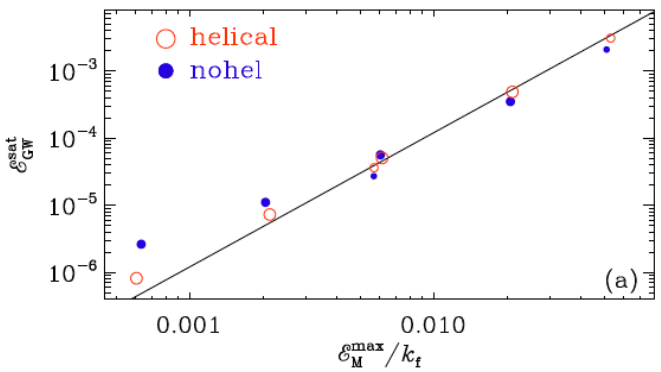

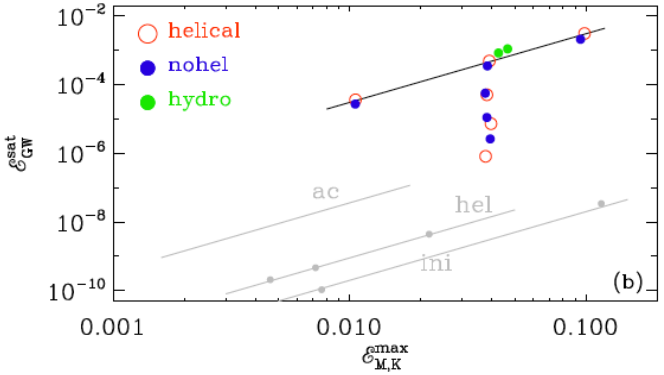

Brandenburg et al (2021) [arXiv:2102.12428]

results

TABLE I: Summary of runs with nonhelical turbulence.

Run	k_f	k_1	f_0	p	τ	$\mathcal{E}_M^{max}$	$\mathcal{E}_{GW}^{sat}$	h_{rms}^{sat}	B [μG]	$h_0^2\Omega_{GW}(f)$	h_c
noh1	2	0.3	1.9×10^{-1}	1.0	16	3.83×10^{-2}	3.53×10^{-4}	4.83×10^{-2}	0.78	1.09×10^{-8}	4.83×10^{-14}
noh2	6	1	6.0×10^{-2}	1.0	4.5	3.75×10^{-2}	5.61×10^{-5}	7.06×10^{-3}	0.78	1.73×10^{-9}	7.07×10^{-15}
noh3	20	3	2.3×10^{-2}	1.3	2.0	3.81×10^{-2}	1.11×10^{-5}	1.15×10^{-3}	0.78	3.44×10^{-10}	1.15×10^{-15}
noh4	60	10	1.0×10^{-2}	1.4	0.43	3.93×10^{-2}	2.62×10^{-6}	1.65×10^{-4}	0.79	8.10×10^{-11}	1.65×10^{-16}
noh5	2	0.3	1.0×10^{-1}	—	—	1.06×10^{-2}	2.70×10^{-5}	1.40×10^{-2}	0.41	8.37×10^{-10}	1.40×10^{-14}
noh6	2	0.3	3.0×10^{-1}	—	—	9.48×10^{-2}	2.08×10^{-3}	1.02×10^{-1}	1.2	6.42×10^{-8}	1.02×10^{-13}
noh7	6	1	2.0×10^{-2}	—	—	4.63×10^{-3}	6.56×10^{-7}	8.10×10^{-4}	0.27	2.03×10^{-11}	8.11×10^{-16}
noh8	6	1	1.0×10^{-1}	—	—	8.90×10^{-2}	3.89×10^{-4}	1.67×10^{-2}	1.2	1.20×10^{-8}	1.67×10^{-14}

TABLE II: Similar to Table I, but for helical turbulence.

Run	k_f	k_1	f_0	p	τ	$\mathcal{E}_M^{max}$	$\mathcal{E}_{GW}^{sat}$	h_{rms}^{sat}	B [μG]	$h_0^2\Omega_{GW}(f)$	h_c
hel1	2	0.3	1.9×10^{-1}	0.67	100	3.90×10^{-2}	4.85×10^{-4}	4.33×10^{-2}	0.79	1.50×10^{-8}	4.33×10^{-14}
hel2	6	1	5.6×10^{-2}	0.67	20	3.81×10^{-2}	5.05×10^{-5}	4.69×10^{-3}	0.78	1.56×10^{-9}	4.69×10^{-15}
hel3	20	3	2.0×10^{-2}	0.67	4.0	3.96×10^{-2}	7.26×10^{-6}	6.66×10^{-4}	0.80	2.24×10^{-10}	6.66×10^{-16}
hel4	60	10	6.5×10^{-3}	0.67	0.50	3.76×10^{-2}	8.15×10^{-7}	7.18×10^{-5}	0.78	2.52×10^{-11}	7.18×10^{-17}
hel5	2	0.3	1.0×10^{-1}	—	—	1.06×10^{-2}	3.61×10^{-5}	1.08×10^{-2}	0.41	1.12×10^{-9}	1.08×10^{-14}
hel6	2	0.3	3.0×10^{-1}	—	—	9.85×10^{-2}	3.07×10^{-3}	1.12×10^{-1}	1.3	9.49×10^{-8}	1.12×10^{-13}
hel7	6	1	2.0×10^{-2}	—	—	4.93×10^{-3}	8.33×10^{-7}	6.26×10^{-4}	0.28	2.58×10^{-11}	6.26×10^{-16}
hel8	6	1	1.0×10^{-1}	—	—	1.20×10^{-1}	5.09×10^{-4}	1.59×10^{-2}	1.4	1.57×10^{-8}	1.59×10^{-14}

Brandenburg et al (2021)
[arXiv:2102.12428]

results

$$\mathcal{E}_{\rm M}(t) = \mathcal{E}_{\rm M}^{\rm max}\,(1+\Delta t/\tau)^{-p}$$

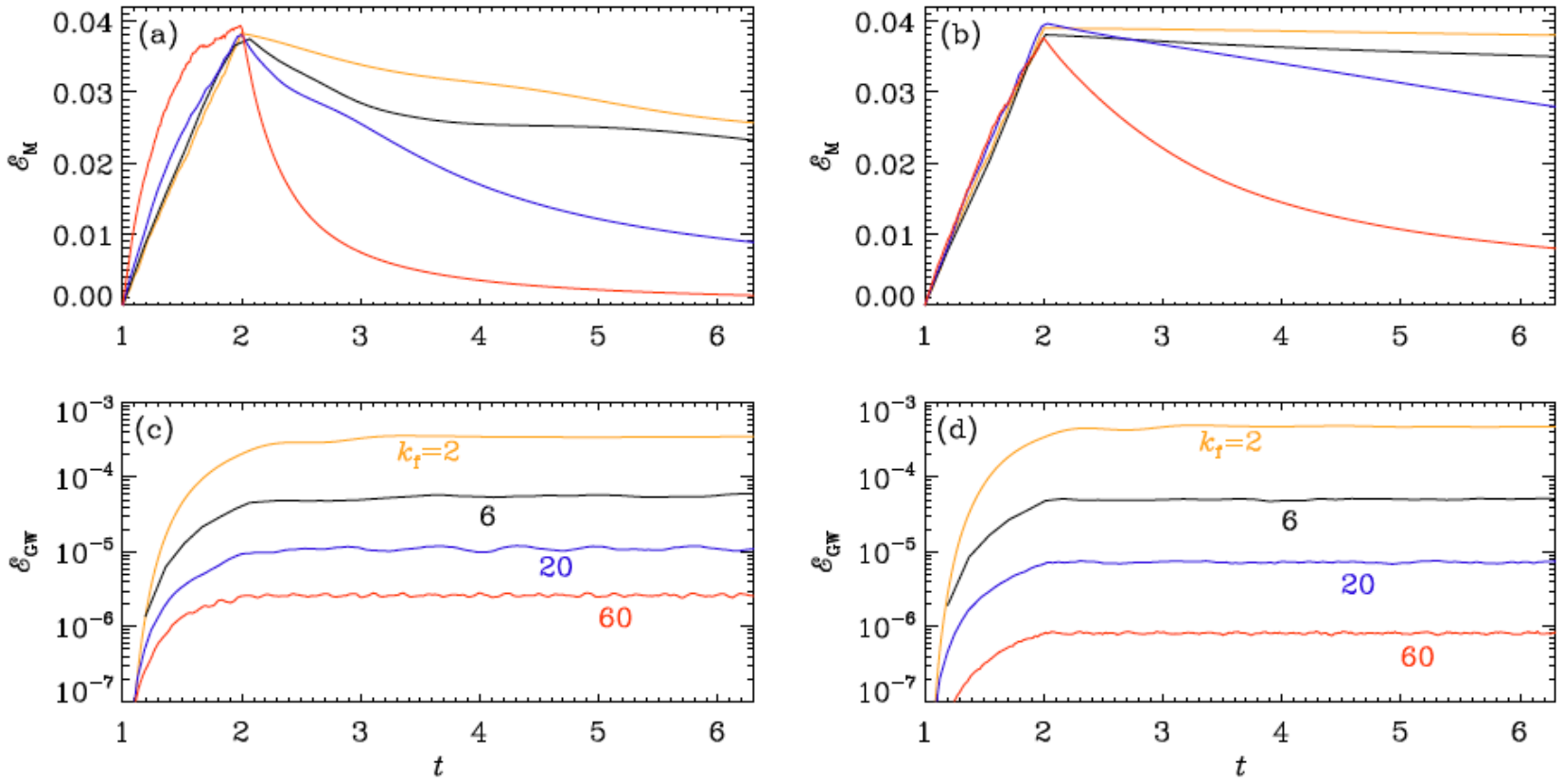

Evolution of $E_M(t)$ and $E_{GW}(t)$ for nonhelical (left) and helical (right) cases. Orange, black, blue, and red are for k_f = 2, 6, 20, and 60, respectively.

Brandenburg et al (2021)
[arXiv:2102.12428]

results

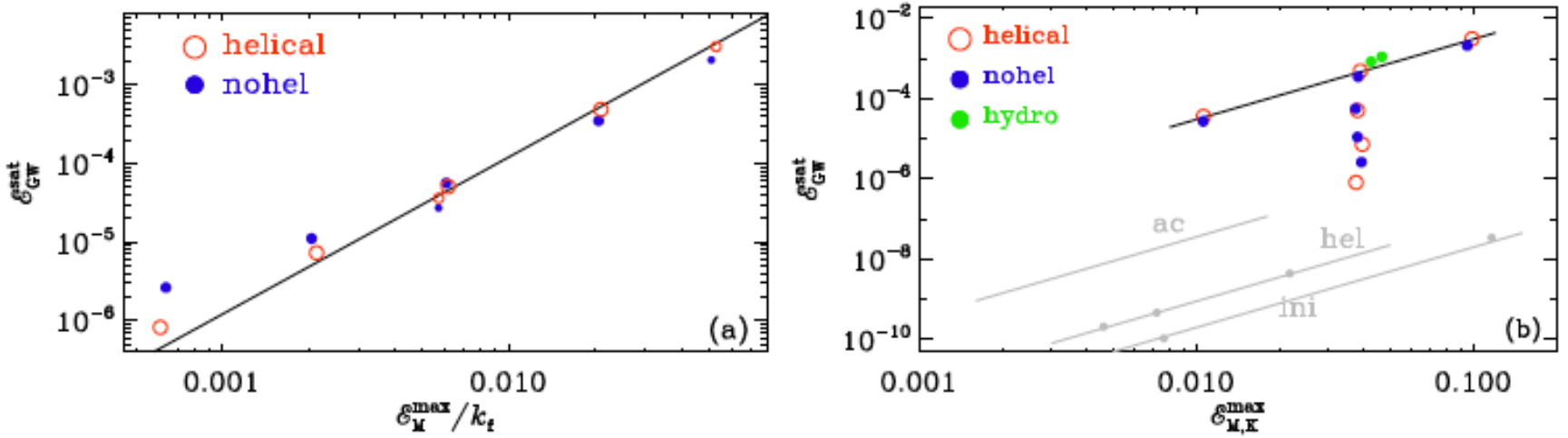

FIG. 4: (a) $\mathcal{E}_{\rm GW}$ versus $\mathcal{E}_{\rm M}/k_{\rm f}$; the straight line shows $\mathcal{E}_{\rm GW} = 5.2\times10^{-4}\,(\mathcal{E}_{\rm M}/k_{\rm f})^{1/2}$. (b) Positions of our runs in a diagram showing $\mathcal{E}_{\rm GW}^{\rm sat}$ versus $\mathcal{E}_{\rm M}^{\rm max}$. For orientation the old data points of the Ref. [73] are shown as gray symbols. The open red (filled blue) symbols are for the helical (nonhelical) runs. The green symbols refer to the two hydromagnetic runs of Table III.

TABLE III: Comparison of nonhelical magnetic turbulence (mag) with irrotational (irro) and vortical (vort) turbulence.

Type	f_0	ν	$\mathcal{E}_{\rm M}^{\rm max}$	$\mathcal{E}_{\rm GW}^{\rm sat}$	$h_{\rm rms}^{\rm sat}$	B [μG]	$h_0^2\Omega_{\rm GW}(f)$	$h_{\rm c}$
magnetic	1.9×10^{-1}	5.0×10^{-5}	3.83×10^{-2}	3.53×10^{-4}	4.83×10^{-2}	0.78	1.09×10^{-8}	4.83×10^{-14}
vortical	3.8×10^{-1}	1.0×10^{-2}	4.21×10^{-2}	8.81×10^{-4}	8.26×10^{-2}	0.82	2.73×10^{-8}	8.27×10^{-14}
irrotational	7.0×10^{-1}	2.0×10^{-2}	4.26×10^{-2}	8.30×10^{-4}	7.95×10^{-2}	0.83	2.57×10^{-8}	7.96×10^{-14}

Brandenburg et al (2021)
[arXiv:2102.12428]

results

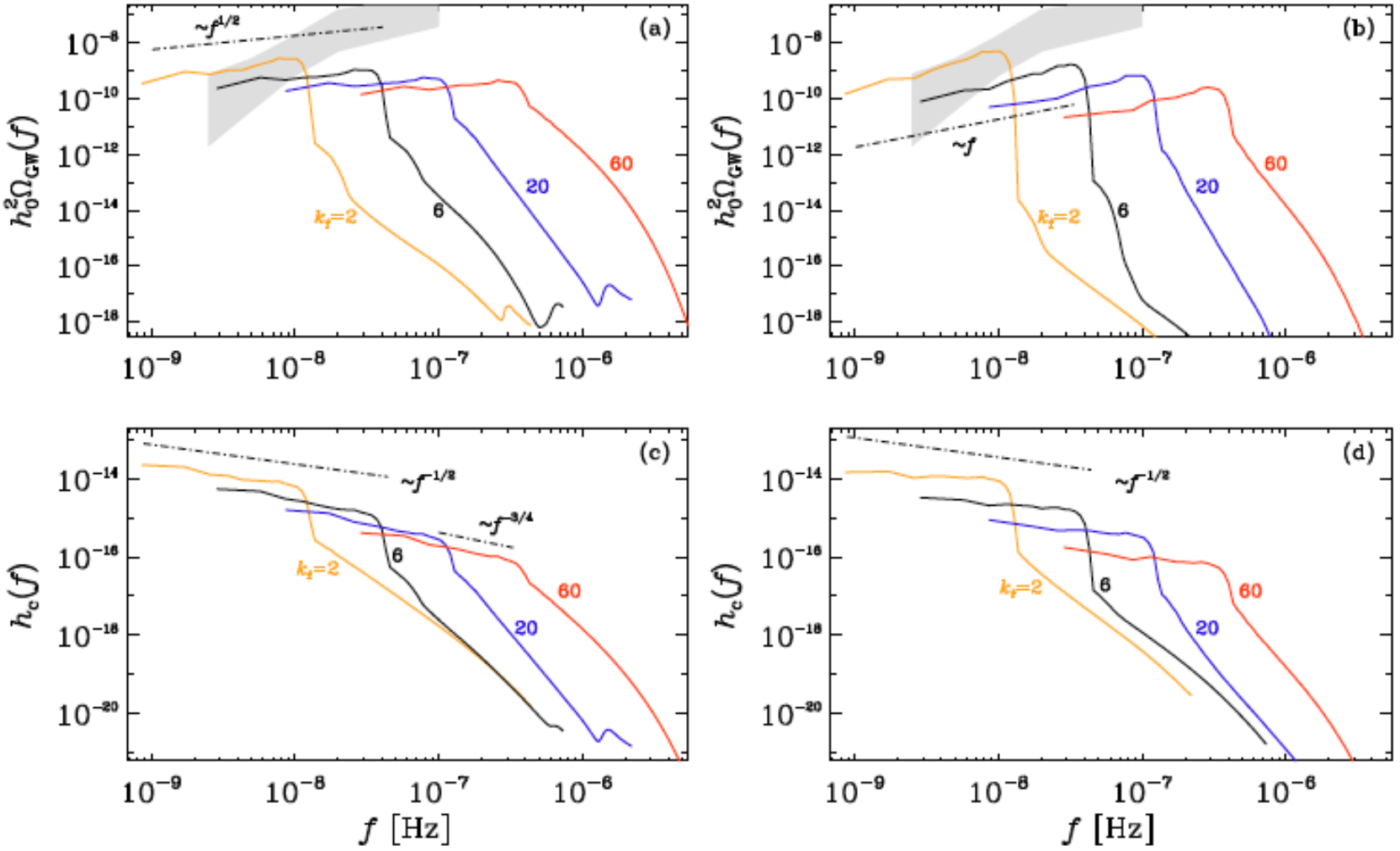

FIG. 5: $h_0^2\Omega_{GW}(f)$ and $h_c(f)$ at the present time for all four runs presented in Table I, for the nonhelical (left) and helical (right) runs. The 2σ confidence contour for the 30-frequency power law of the NANOGrav 12.5-year data set is shown in gray.

Brandenburg et al (2021) [arXiv:2102.12428]

results

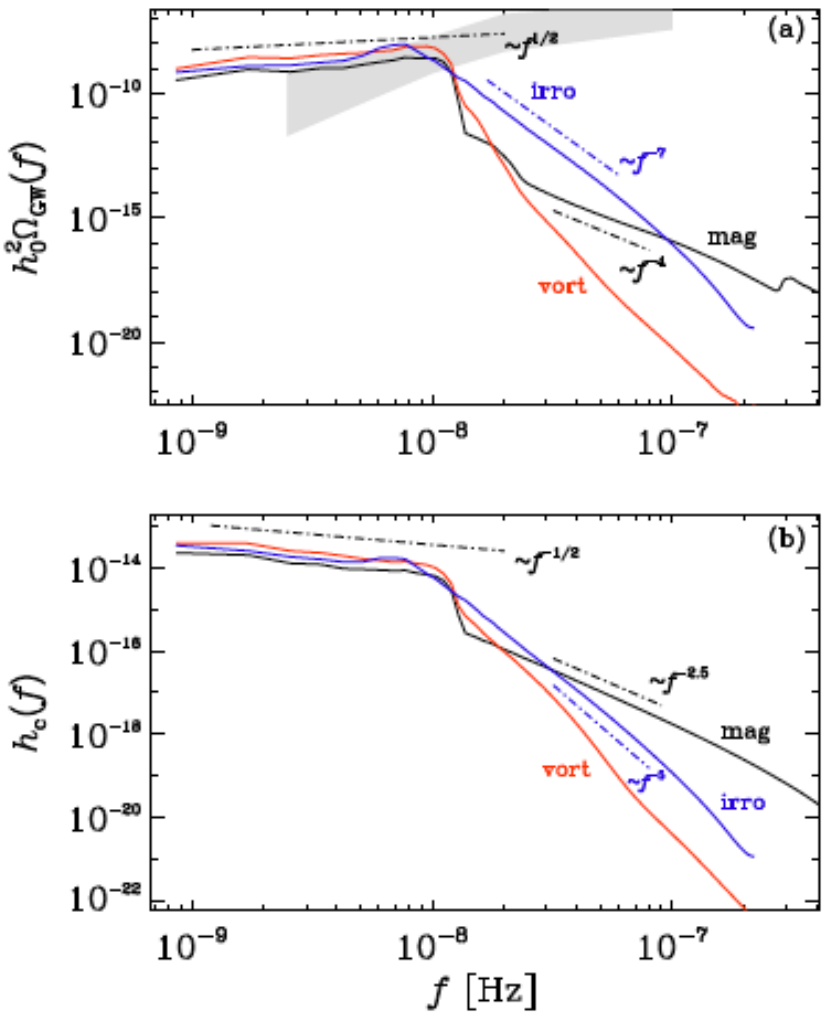

FIG. 7: Similar to Fig. 5, but comparing vortical (red) and irrotational turbulence (blue) with MHD turbulence (black).

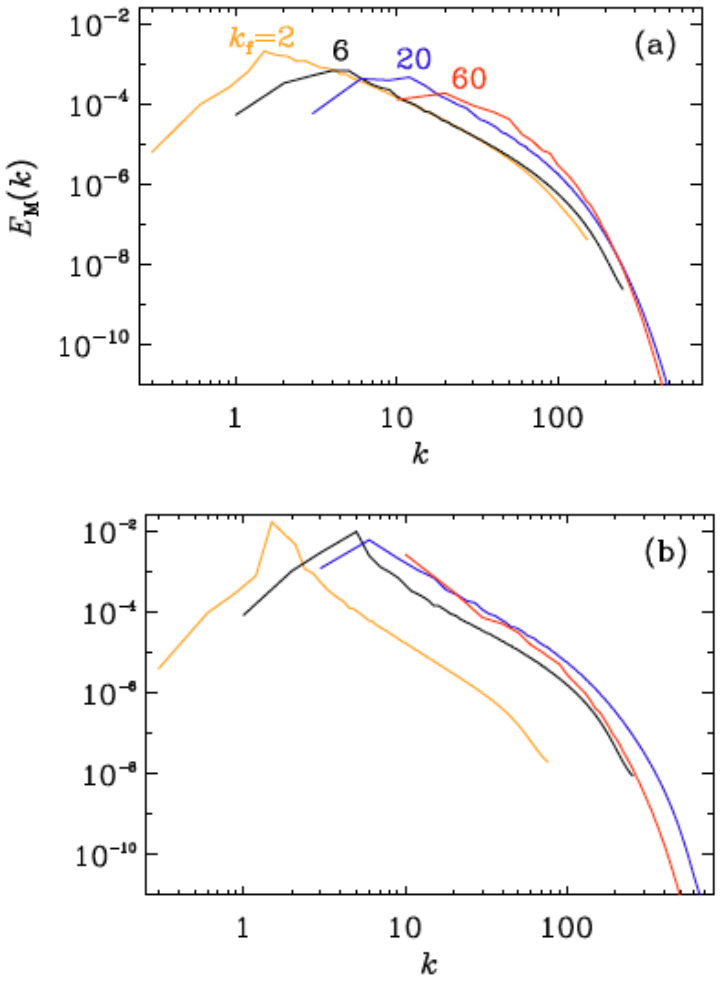

Magnetic energy spectra for the (a) nonhelical and (b) helical cases

Brandenburg et al (2021) [arXiv:2102.12428]

conclusions

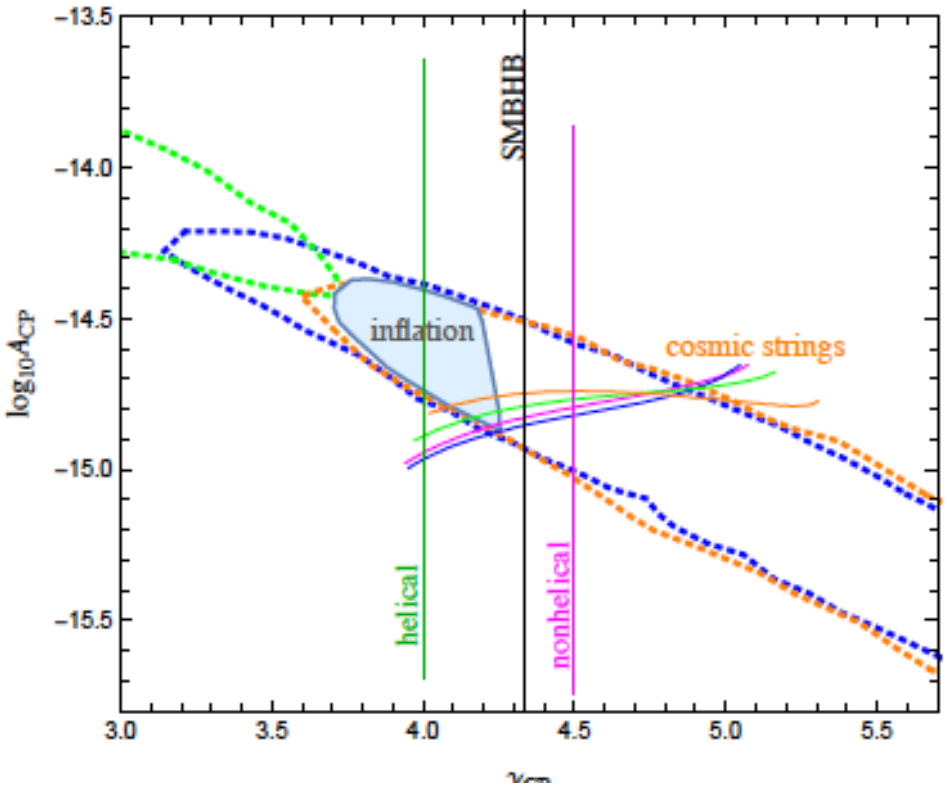

Hydrodynamic and MHD Turbulence @ QCD scale (this work):

- $f < f_{peak}$: $\gamma \approx 4$ (helical), $\gamma \approx 4.5$ (non-helical)
- $f > f_{peak}$: $\gamma \approx 12$ (kinetic), $\gamma \approx 9$ (mhd)

Credit: Emma Clarke

- ✓ ***Magnetic stress from hydrodynamic and MHD turbulence with scales comparable to the cosmological horizon scale at the QCD transition can drive GWs in the range accessible to NANOGrav if the magnetic energy density is 3-10% of the radiation energy density.***
- ✓ ***Our work has led to new insights regarding the possibility of using an observed GW spectrum for making statements about the nature of the underlying turbulence in the early universe. One is the already mentioned slope of the subinertial range spectrum. Another is the position of the peak of the spectrum***
- ✓ ***The specific features of the spectrum near the peak are different for helical and nonhelical turbulence. This could, in principle, give information about the presence of parity violation, when would also lead to circularly polarized GWs.***

Thank you for listening!
Questions?

My thanks to

- ✓ Organizers
- ✓ My collaborators
- ✓ Shota Rustaveli National Science Foundation of Georgia
- ✓ Swedish National council

FR18-1462